Performance Analysis of Passive Resonance Circuit Breakers in HVDC Systems

Sadegh Ghavami, Ali A. Razi-Kazemi, *Senior Member, IEEE*, K. Niayesh, *Senior Member, IEEE*

***Abstract*-- Passive resonance breaker is employed based on the creation an artificial current zero crossings in the transfer switch in the promising HVDC networks. The interruption process physically depends on the instability of the switching arc and interaction with the resonant circuit. In addition, the stored energy in the breaker can influence on a successful interruption. This paper presents a comprehensive insight into the operation of passive resonance breaker (PRB) and the arc instability during the interruption process. A black-box arc model based on the Schwarz as the model with a high degrees of freedom and the genetic algorithm (GA) as a heuristic optimization has been presented to follow the characteristics of the static and quasi-static arc regarding the oscillation frequency of the interruption current. Subsequently, the dynamic behavior of the PRB has been quantified based on the state-space approach along with an accurate dynamic arc model to follow a wider frequency range of the arc current. The results are indicated that the amplification coefficient alone is insufficient to determine the interruption capability. Therefore, this paper attempts to quantitatively determine the interruption capability curve by introducing criteria, such as Δt_{PZ} (peak to zero time-interval), di_{arc}/dt_{CZ}^{-} and du_{arc}/dt_{CZ}^{+} to obtain the origins of the interruption failures probability with respect to the interruption limits for gas blast circuit breakers (CBs).**

***Index Terms*-- arc model, passive resonance, black-box model, HVDC circuit breaker**

I. Introduction

INCREASING the role of off-shore wind power resources and power controllability in HVDC systems, long-distance power transmissions alongside asynchronous power grid connections lead to the popularity of HVDC systems. In order to comply with protection constraints, circuit breakers (CBs) play a critical role in these networks specifically in multi-terminal HVDC networks [1]. Direct-current interruption is highly challenging due to the inherent lack of current zero-crossing in DC systems [2]. Accordingly, different current-interrupter topologies have been developed in [3]–[5] with some advantages and drawbacks.

Sadegh Ghavami is with The Electrical Engineering Department, K. N. Toosi University of Technology, 16315 Tehran, Iran (e-mail: sadegh.ghavami@email.kntu.ac.ir).

A. A. Razi-Kazemi is with Electrical Engineering Department, K. N. Toosi University of Technology, 16315 Tehran Iran (e-mail: Razi.Kazemi@kntu.ac.ir).

K. Niayesh is with Department of Electric Power Engineering, Norwegian University of Science and Technology, 7491 Trondheim Norway (e-mail: Kaveh.Niayesh@ntnu.no).

There was considerable interest in active and passive resonance breakers (PRBs) owing to their simple structure [6], [7]. As the requirement of the HVDC point-to-point transmission system is the operation in monopolar mode, the Metal Return Transfer Breaker (MRTB) was introduced in [8]. The motivation of using multi-terminal HVDC increased in the 1980s; consequently, the first prototypes of HVDC air-blast and SF_6 CBs have been employed as the main breaker with different arrangements and minor changes in the nozzle to operate in the higher currents [9]–[12]. Great efforts have been devoted to the investigations dealing with the interaction between DC arc in the mechanical CB and parallel shunt-impedance circuit based on the instability of DC arc [13], [14]. They focused on the change of the arc characteristics by variations in the nozzle geometry. In the last few years, there has been a growing interest in studying the switching arc for modeling the dynamic behavior of DC interruption process [15]–[17]. In addition, many researchers have investigated the variation of the arc characteristics affected by external conditions such as a cooling power and axially blown arcs [18], transverse magnetic field [19], [20], and different gas types [15],[18],[19]. Moreover, researchers revealed that arc could excite the parallel-impedance with a positive amplification coefficient and provide an increasing oscillating current in case of the negative differential resistance of arc (du_{arc}/di_{arc}). However, the differential resistance is negative in the low current range and it becomes zero (flat) or positive in the higher-currents [21]. Therefore, PRBs are unable to interrupt the short circuit current owing to limitations resulted from the arcing nature. Accordingly, they might be applied as the load current breaker or transfer switches in the future HVDC systems [22].

In order to scrutinize the behavior of PRBs, it is necessary to address an accurate arc model owing to its interaction with the resonant circuit as well as the constraints dealing with a successful interruption. Accordingly, the black-box model is a valuable approach to provide a fast running dynamic behavior of the arc in PRBs [23], [24]. The point is that an arc can be described with a static, a quasi-static, or a dynamic characteristic. This paper presents a black-box arc model based on the genetic algorithm (GA) as a heuristic optimization method to identify the arc parameters regarding the sinusoidal (single-frequency) and non-sinusoidal current (multi-frequency) waveforms associated with the characteristics of static, and quasi-static, respectively. As the current can vary within different frequency ranges in PRBs, it is necessary to apply a dynamic arc model for tracking the

behavior of the arc voltage in such a condition. Accordingly, a dynamic arc model using [15] has been added in this approach to investigate the arc voltage. Furthermore, the model has been represented analytically based on the state-space model to clarify the interaction between the arc model and the resonant circuit.

The possibility of re-ignition in the mechanical CBs [9], especially in the future HVDC networks due to the increase in the voltage level can limit the interruption capability. Moreover, there is no standard test dealing with this issue for HVDC CBs [25]-[27]. In addition, previous efforts have focused on the amplification coefficient as a criterion of the interruption capability [13], [14]. In response to the lack of a suitable theoretical study on origins of the interruption failure conditions in PRBs, this paper presents a precise capability curve by introducing Δt_{PZ} (peak to zero time-interval), di_{arc}/dt_{CZ}^{-} *and* du_{arc}/dt_{CZ}^{+} as the criteria of successful interruption.

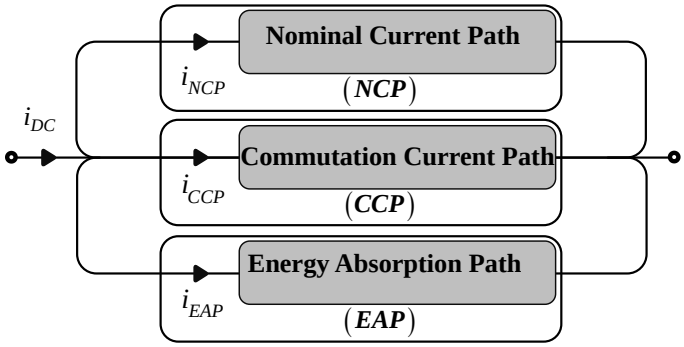

Fig. 1. General scheme of HVDC CB (adapted from [2]).

The manuscript is structured as follows: Section II briefly reviews the basic principles of HVDC CBs and PRBs with special emphasis on the role of arc parameters in the interaction between the electric arc and parallel shunt impedance which leads to a dynamic characteristic for the arc. Section III presents an arc modeling based on the GA as a heuristic optimization method for the identification of the static and quasi-static characteristics of the wall stabilized and free burning arc. Serving the state-space representation for investigating instability of the PRB arc has been provided in section IV. In section V, the interruption capability in different frequency ranges is discussed. Finally, the conclusion is presented in section VI.

II. HVDC CB Basic Principle

HVDC CBs consist of three parallel paths as shown in Fig. 1. The nominal current path (NCP) includes an interrupter with a low on-resistance in the closed position to minimize the conduction losses. It could be addressed through a mechanical breaker, solid-state switches or hybrid approach. In the case of active and passive resonance breakers, it is equipped with a mechanical breaker, while the full solid-state based CBs are employed many solid-state arrays resulting in a high on-state loss. Accordingly, the loss is decreased significantly in the hybrid CB, where few solid-state switches series in a mechanical disconnector are employed.

Commutation current path (CCP) is excited/activated during the current interruption process to provide an artificial zero crossing. While in the active resonance breaker, the current is injected into the main path by a pre-charged capacitor, a negative differential arc resistance creates an oscillation current in the PRBs. Furthermore, in hybrid breakers, the commuted current from NCP is interrupted in the CCP where many solid-state arrays are allocated. Subsequently, the current interruption causes a transient interruption voltage (TIV) across the capacitor(s) of the commutation path or snubber circuit and the main the breaker up to the residual voltage of the surge arrester. Therefore, the current flows through the energy absorption path (EAP) that dissipates the stored energy in system inductance.

A. PRB Basic Principle

The physical basis for the current interruption in PRB depends on the arc-instability. Accordingly, the following conditions should be governed: 1) The current needs to be lower than the maximum current that leads to $du_{arc}/di_{arc}<0$ and 2) the sum of the differential resistance of the arc with the stray resistance r_{res} of the parallel-impedance needs to be negative.

As shown in Fig. 2, the solid line presents the arc voltage u_{arc} as a function of the arc current i_{arc}. It refers to a negative differential resistance in u_{arc}-i_{arc} characteristic of an electric arc. NCP and CCP are considered in this work as shown in Fig. 2. f_{res} ($\frac{\omega_{res}}{2\pi}$) refers to the frequency of the forced current by the resonant circuit.

The impedance of CCP consists of an inductor and a capacitor in series, paralleled to the arc with a negative differential resistance (arc operating point). This results in a growing oscillatory current in the CCP and NCP. The current amplitude is increased with a specific amplification coefficient to reach a current higher than the DC level, which provides a current zero. Subsequently, the arc could be quenched off in the NCP.

B. Arc Phenomena and Black-Box Model

Mayr model is a well-known arc model behavior based on a first-order ordinary differential equation in time-domain called the energy balance equation as (1):

$$\dot{g}_{arc} = \frac{1}{\tau}\cdot\left(\frac{{i_{arc}}^2}{P} - g_{arc}\right) \tag{1}$$

Since the arc is inherently non-linear, to achieve a better correlation between the measured values and calculations, the cooling power (P) and thermal inertia (τ) as free functions of conductance (g_{arc}) could be described as follows:

$$P(g_{arc}) = P_0 g_{arc}^{\alpha} \tag{2}$$

$$\tau(g_{arc}) = \tau_0 g_{arc}^{\beta} \tag{3}$$

All these assumptions lead to the fact that (1) becomes a non-linear description of the arc conductance as a state variable.

The variations in the current during the interruption result in a change in the arc conductivity, cross-section, and temperature. There is an interaction between instantaneous power heating (Joule heating) and cooling power (due to radiation, laminar and turbulent convection, and conduction) during an interruption.

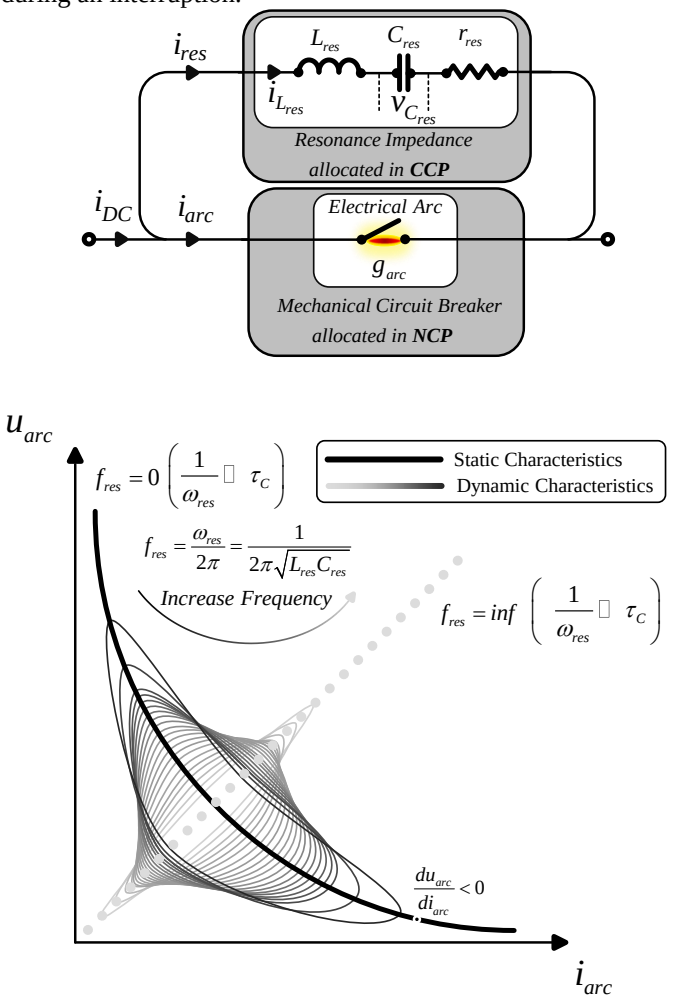

Fig. 2. Static and Dynamic characteristics of the arc with Hysteresis loops for different frequency AC superimposed current breaker (adapted from [16]).

In addition, the dynamic behavior of the arc depends on the arc time constant, or time constant. It plays the main role in transferring arc energy to the surrounding environment during the interruption process.

Fig. 2 shows the impact of the static characteristic of the arc (solid black-line) and dynamic characteristics of the arc (gray faded-lines) resulting from the resonant circuit. As there is an inherent hysteresis manner between arc current and arc heating (or conductivity), the u_{arc}-i_{arc} characteristic of an arc is similar to those demonstrated in Fig. 2, which is dependent on the frequency of the arc current. For better clarification, the role of arc parameters is represented by a critical time constant (τ_C) [12], which are explained in details in the following:

I) The period of angular frequency much greater than the critical time constant ($\frac{1}{\omega_{res}} \gg \tau_C$)

Arc conductance can rapidly follow the current variations. In this condition, instantaneous power heating to the arc equals the instantaneous cooling power and the arc exhibits a negative differential resistance characteristic. The current fluctuations change the plasma column and ionization level resulting in variation in the conductivity. Consequently, the arc voltage follows the current with the u_{arc}-i_{arc} characteristic as shown by the solid line in Fig. 2. As the arc can maintain equilibrium with the current change, the static arc characteristics are followed by a very small period of the current oscillating. This condition is most often practically met in the case of power-frequency current.

II)The period of angular frequency much lower than the critical time constant ($\frac{1}{\omega_{res}} \ll \tau_C$)

In this situation, the arc conductance cannot track the current variations all the way. Therefore, the arc conductance will not change during the period of the current oscillation. The ionization could not follow the high-frequency current, any change in the arc current results in a similar change in the arc voltage as shown by the dotted line in Fig. 2. Arc current and voltage are in-phase and the arc behaves like a pure positive resistance that leads to a damping oscillating current.

III) The period of angular frequency lies adjacent to the critical time constant ($\frac{1}{\omega_{res}} \cong \tau_C$)

Once the period of the current oscillating approaches the critical time constant, an interesting and somewhat unusual condition occurs. In this case, the ionization level, arc conductivity, and arc voltage could track the changes in the current with a time delay. The time lag between the arc current and voltage leads to the increment of the arc voltage in comparison with the statics curve in initial steps and the decrease of the voltage in returning the current as shown by the gray lines in Fig. 2.

III. Validation and Verification: Arc Modeling as an Optimization Problem

This section presents the proposed approach to find out the

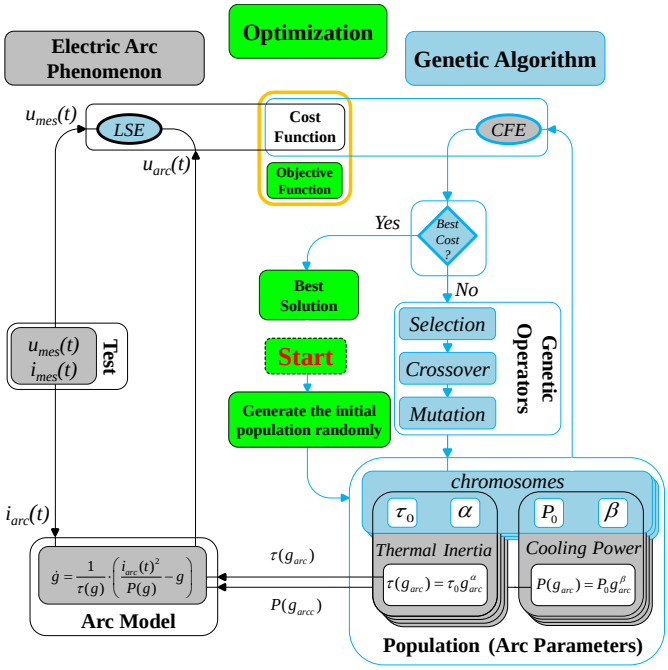

Fig. 3. The Flow chart of the proposed approach with the use of GA algorithm

dynamic model of the arc using GA. Fig. 3 presents the outline of the approach including three sections, i.e. "electric arc phenomenon", "Genetic Algorithm" and "optimization".

The parameters consist of P_0, τ_0, α and β based on (1)-(3). The "electric arc phenomenon" has been run based on these equations and the initial conditions for the parameters. The section "Genetic Algorithm" and "Optimization" try to find the optimum solution through the least square technique (LSE) and the cost function evaluation (CFE) step.

The LSE is defined as the sum of the square difference between the measured arc voltage (u_{mes}) and the analytically predicted arc voltage ($u_{arc}(t)$) as a response of the arc model calculated in this step.

The quasi-static and static characteristics of the arc are estimated for an excitation current with frequency content (non-sinusoidal) and single-frequency (sinusoidal) toward wall-stabilized and free burning arc, respectively.

A. Genetic Algorithm framework

The GA is a well-known metaheuristic optimization algorithm based on the mechanism of the natural genetics of Mendel's theory and natural evolution in the Darwinian theory. The GA search starts with a collection of solutions called population that are initially generated randomly. This population can be seen as a collection of chromosomes that represent the arc parameters which are interpolated to the arc model equation under consideration [28].

The fitness of each chromosome assessed via CFE respecting that the fitter chromosomes survive into the next generation. GAs manipulate fitness value associated with individuals of the population.

The simplest form of GAs in its standard scheme is presented in Fig. 3. The most significant step of the algorithm is the generation of a new population of individuals through the application of the genetic operators: selection, crossover, and mutation. These are applied for the production of the new chromosomes as the next generation population.

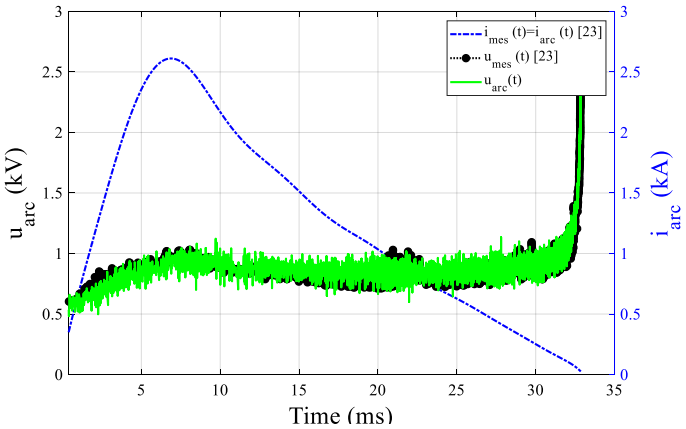

Fig. 4. Wall-stabilized arc calculated voltage $u_{arc}(t)$ and externally measurement waveforms given [23]

Selection refers to an individual's selection for a mating that defines the chromosomes that survive to produce the population in the next generations. Crossover is a reproduction operator that takes valuable genetic information from two individuals (parents) and recombines it to produce a new individual (offspring). Mutation changes randomly one or more genes in the parent chromosome with a small mutation rate P_m. The purpose of mutation is to induce some diversity into the population to prevent the GA search converging to a local optimum or getting trapped in it [28].

B. Arc Parameter Determination and Model Validation

The black box arc models predict the dynamic behavior of the arc during the thermal period. The behavior of the arc-network has been governed through a first-order ordinary differential equation (1), the so-called energy balance equation. To determine the arc characteristics, the measurement of an arc voltage $u_{mes}(t)$ and arc current $i_{mes}(t)$ conducted in a 23-mm diameter nozzle in [23] for wall stabilized arc (non-sinusoidal current waveform) as well as a 4-mm gap distance in [24] for a free burning horizontal arc (sinusoidal current waveform) have been employed in the model. Noteworthy is that the contact shape and material does not play an important role in this study, since the utilized arc is a hot gas column and the vaporization of the metal is low [29]. With respect to the general energy balance equation (1), the estimated arc model would be identified only by the arc time constant τ_0 and cooling power constant P_0 in the case of $\alpha=0$ and $\beta=0$. On the contrary, in the case of $\alpha\neq0$ and $\beta\neq0$, it would be determined by the $\tau(g_{arc})$ and $P(g_{arc})$ as the free functions of conductance. It leads to a nonlinear description known as the Schwarz arc equation.

The required parameters of the arc as an energy reservoir need to be identified. The Schwarz arc equation has been selected owing to four free parameters in representing of the arc behavior, which is more precise than two free parameters in the case of $\alpha=0$ and $\beta=0$.

To implement the proposed approach, the GA search algorithm starts by randomly generating the initial population (parameters) and the simulated arc-voltage waveform $u_{arc}(t)$

acquired by solving the differential equation of the provided arc model. The objective of the optimization problem is to determine the arc model parameters by minimizing the LSE as a cost function as follows:

$$Cost\ Function=LSE=\sum_{t=1}^{n}\left|u_{mes}(t)-u_{arc}(t)\right|^{2} \quad (4)$$

The arc model has adjustable parameters, which are transferred from GA in the CFE step. In each iteration, a

TABLE I
GA AND ARC PARAMETERS EVALUATION FOR NON-SINUSOIDAL CURRENT

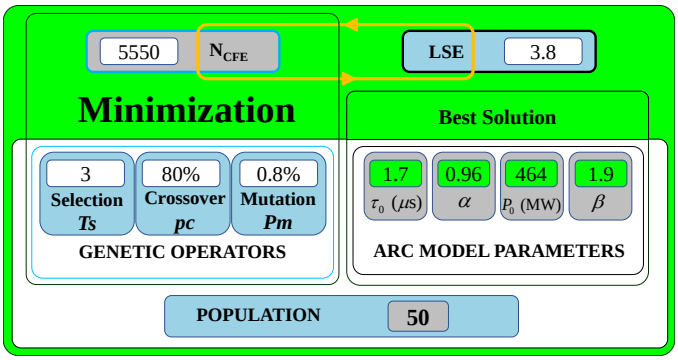

series of candidate solutions generated by the genetic operators (Mutation, Crossover, and Selection) are imported into the cost function to select the best solution. The algorithm terminates when the satisfactory number of CFE (N_{CFE}) or the maximum iterations has been reached.

The arc voltage response $u_{arc}(t)$ (see Fig. 4 and Fig.5: green solid line) of the numeric results for the Schwarz model and measured arc voltage $u_{mes}(t)$ (black circles point) and measured arc current $i_{mes}(t)$ (blue dashed line) are shown in Fig. 4 and Fig. 5. Considering the stochastic fluctuations of the arc voltage by Gaussian noise with zero mean value in the process of parameters estimation, which makes the model close to the real world and robust to fluctuations. The identified arc parameters based on GA search after 100 iterations are presented in Table I and Table II.

As this nonlinear problem might stick in local minimum points, the genetic operators employed in this approach reduces the possibility of these difficulties.

To verify the applicability of the proposed approach in a single frequency case, a comparison has been conducted via experimental arc voltage in [24] as illustrated in Fig. 5. As can be seen, the arc voltage obtained by the GA is in good agreement with the recorded voltage in [24].

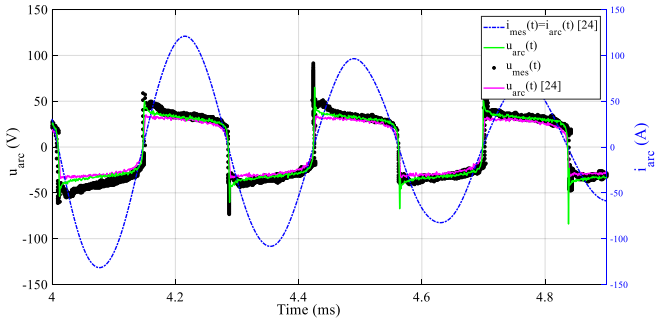

Fig. 5. Comparison between the free-burning arc voltage measurement, the calculated arc voltage $u_{arc}(t)$ by GA, and the reported result in [24]

TABLE II
GA AND ARC PARAMETERS EVALUATION FOR SINUSOIDAL CURRENT

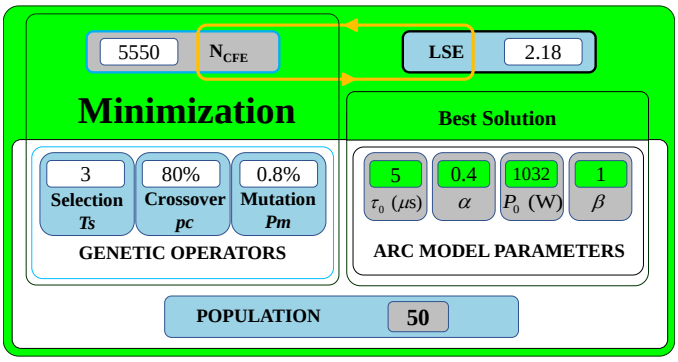

IV. Instability of the Arc in PRB (State Equations)

To develop a general numerical procedure for investigating the instability of the arc in PRB, the electric equivalent circuit, shown in Fig. 2, is employed to represent the analytical model. The arc is assumed to be stabilized across fixed contacts, i.e., the arc elongation and contact separation are not considered, and the other external conditions like blowing gas flow remain constant. The arc discharge process is characterized by the Schwarz differential equations (1)-(3) as shown in Fig. 2 by conductance g_{arc}.

The state-space approach has been employed for the analytical evaluation of the interruption process. Arc conductance describes the basic characteristic of the arc as an energy reservoir and is obtained by solving the differential equations (1). Thereby, it could be a state variable. Accordingly, the state variables are the voltage across the capacitor $x_1(t)=v_{Cres}$, resonance current through the inductor $x_2(t)=i_{Lres}$, and the arc conductance $x_3(t)=g_{arc}$. The state space model of the PRB is expressed as follows:

$$f_1=\dot{x}_1(t)=\frac{dv_{Cres}}{dt}=\frac{1}{C_{res}}i_{Lres} \quad (5)$$

$$f_2=\dot{x}_2(t)=\frac{di_{Lres}}{dt}=-\left(\frac{r_{res}}{L_{res}}+\frac{1}{L_{res}g_{arc}}\right)i_{Lres}-\frac{v_{Cres}}{L_{res}}+\frac{i_{DC}}{L_{res}g_{arc}} \quad (6)$$

$$f_3=\dot{x}_3(t)=\frac{dg_{arc}}{dt}=\frac{1}{\tau}\cdot\left(\frac{(i_{DC}-i_{Lres})^2}{P}-g_{arc}\right) \quad (7)$$

where $f_i(x_i,i_{DC},t)$ is a nonlinear and time-dependent function of the state variables and the interruption current.

For investigating the instability of the arc and its interaction with parallel-impedance as the resonance circuit, the standard form for the state-space representation has been used to describe system dynamics in this section. In order to calculate the state matrix, A, it has been assumed that the system operates around an equilibrium point, i.e., the arc is in the steady-state. Therefore, cooling power equals the arc input power $P = u_{arc}i_{arc}$, and all variables at the operation point are known: $g_{arc} = i_{arc}/u_{arc}$ and $i_{arc} = i_{DC}$. The linearization is performed based on the expansion of nonlinear function(s) f_i

into a Taylor series expansion around the operating point. The state matrix, *A*, is accomplished by taking all partial derivatives of f_i and neglecting the higher-order terms that lead to forming the Jacobin matrix J^* as shown in equation (8).

$$A = J^* = \begin{pmatrix} \partial f_1/\partial i_{L_{res}} & \partial f_1/\partial v_{C_{res}} & \partial f_1/\partial g_{arc} \\ \partial f_2/\partial i_{L_{res}} & \partial f_2/\partial v_{C_{res}} & \partial f_2/\partial g_{arc} \\ \partial f_3/\partial i_{L_{res}} & \partial f_3/\partial v_{C_{res}} & \partial f_3/\partial g_{arc} \end{pmatrix}$$

$$= \begin{pmatrix} \frac{1}{C_{res}} & 0 & 0 \\ -\frac{r_{res}}{L_{res}} - \frac{1}{g_{arc}L_{res}} & -\frac{1}{L_{res}} & -\frac{i_{DC}}{g_{arc}^2 L_{res}} \\ \frac{-2i_{DC}}{P_0\tau_0 g_{arc}^{\alpha+\beta}} & 0 & -\frac{(\alpha+\beta)(i_{DC})^2}{P_0\tau_0 g_{arc}^{\alpha+\beta+1}} - \frac{(1-\beta)}{\tau_0 g_{arc}^{\beta}} \end{pmatrix} \quad (8)$$

The eigenvalues of state matrix *A* are calculated via (9):

$$\Delta(s) = det(SI - A) = 0 \quad (9)$$

The system is stable if all eigenvalues of J^* acquire negative real parts at the equilibrium point. Therefore, if at least one of the eigenvalues gets a positive real part, the resonance current i_{Lres} grows from the equilibrium point.

The required condition for arising instability is that the negative dynamic resistance needs to be lower than the stray resistance in the equilibrium point: $du_{arc}/di_{arc} < -r_{res}$.

The characteristic equation (9) for matrix *A* is a polynomial of *s* (3th order). Therefore, it should contain three roots in which only complex roots are remarkable. Once two roots of the characteristic equation are complex conjugate, the resonance current gets oscillating. Furthermore, if the real part of the complex solutions α_{res} is positive, it deviates from the equilibrium point and grows with a specific amplification coefficient. Therefore, a general solution of the characteristic equation of (9) can be given as follows:

$$(s-\alpha)\cdot(s-\alpha_{res}-j\omega_{res})\cdot(s-\alpha_{res}+j\omega_{res}) = 0 \quad (10)$$

By numerical integration of the linearized characteristic equation (10), the analytical evaluation of the frequency ($f_{res} = \omega_{res}/2\pi$) and the amplification coefficient α_{res} against changes in the value of the parallel-impedance parameters has been obtained as two significant affecting parameters in PRBs.

Accordingly, the model has been applied to interrupt the current of 1.2 kA. It is the maximum threshold of the current interruption capability based on the available reported arc characteristics for a chamber blown arc with 15.5 bar in a 25 mm diameter nozzle in [15]. In order to precisely investigate the PRBs, a dynamic arc model that could track a wider frequency range is necessary. The accurate dynamic arc characteristic in the mentioned situation is represented by $P(g_{arc}) = 1.03 g_{arc}^{0.5}$ (MW) and $\tau(g_{arc}) = 8.3 g_{arc}^{0.4} (\mu s)$ that reported in [15].

Fig. 6 presents the sensitivity analysis of the amplification coefficient (α_{res}) and the frequency of complex conjugate roots (f_{res}) against the parameters of the resonance circuit dealing with unstable conditions. As it can be seen, the frequency generally increases by decreasing either capacitor or inductor as the main elements of the parallel-impedance in the resonance circuit.

The bottom plot in Fig. 6 indicates that the amplification coefficient finds its maximum in a value of the inductor, less than 100 μH. However, a higher value of the inductor leads to

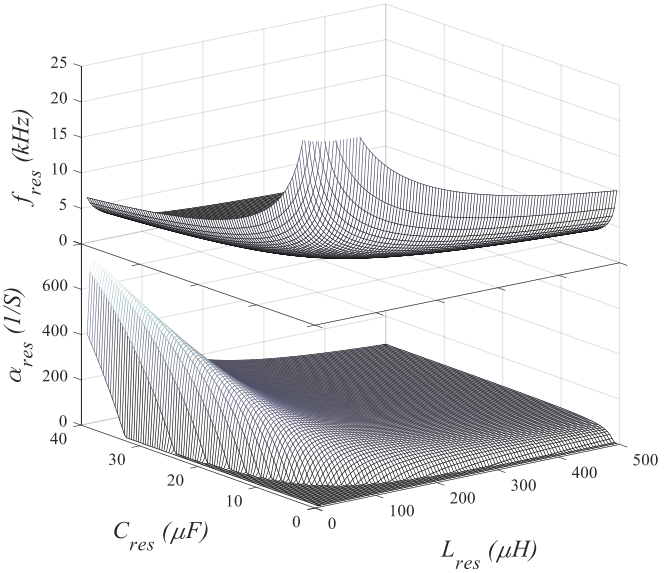

Fig. 6. The frequency and amplification coefficient corresponds with the complex conjugate roots by variation the inductor and capacitor in parallel-impedance

a decrease in the amplification coefficient and a higher oscillation frequency.

In PRB, high oscillation frequency produces the larger current gradients and causes a shortened lag between the arc voltage and current. Noteworthy is that the interrupter cost gives consideration to the capacitor cost; consequently, a large capacitor would not be desirable.

V. INTRODUCING THE CAPABILITY CURVE FOR DIFFERENT FREQUENCY RANGES

The amplification coefficient α_{res} can specifically be defined as the growth rate of resonance current that provides zero-crossing for the current flow through an interrupter. Moreover, there is a time limitation to provide the required forced-current for the interruption. Previous efforts in [13], [14] mostly defined the amplification coefficient as an index of the interruption capability, despite; no attempt was made to quantify the correlation between this growth rate and resonance frequency and interruption capability. More precisely, a successful interruption could happen considering both the frequency of the oscillating current and the required amplification coefficient (α_{PZC}) as discussed in this paper.

The interruption limits for gas blast mechanical CB describe the ability of a CB to fulfill a given switching duty. The current before zero-crossings governs the conductance of the plasma column in a few microseconds before the current zero. In addition, to avoid thermal re-ignition, it is necessary to quickly decrease the arc conductance from very high values to near zero at CZ [30].

In the case of PRB, with respect to the high peak current (i_{arc}^{peak}), the probability of successful interruption at CZ closely corresponds to the following key criteria:

di_{arc}/dt_{CZ}^{-}: time derivative of the current before CZ

du_{arc}/dt_{CZ}^{+}: time derivative of the voltage after CZ

Consequently, the amplification coefficient could not provide helpful information associated with a successful interruption as well as the possibility of a re-ignition during switching arc duty.

In the present effort, the time interval between the time of occurrence of CZ (t_{CZ}) and peak current (t_{peak}) is defined as an essential criterion via (11). It can help to determine the probability of thermal re-ignition in the PRBs.

$$\Delta t_{PZ} = t_{CZ} - t_{peak} \tag{11}$$

To give an illustration, the simulation of interruption of a 1.2 kA DC current is presented in Fig. 7. The simulations are implemented in PSCAD applying a time step of 1 ns and break time at 4 ms. The arc voltage excites the parallel-impedance by $C_{res} = 20\ \mu F$ and $L_{res} = 150\ \mu H$. In addition, the proposed criteria are magnified in Fig. 7.

To evaluate the criteria, capacitor and inductor values are set up for different excitation frequencies. Fig. 8 serves the criteria regarding the changes in the time interval Δt_{PZ} as a function of the resonance frequency.

The defined time interval Δt_{PZ} can represent the arc voltage lag to the current and make a connection with the arc time constant τ_0.

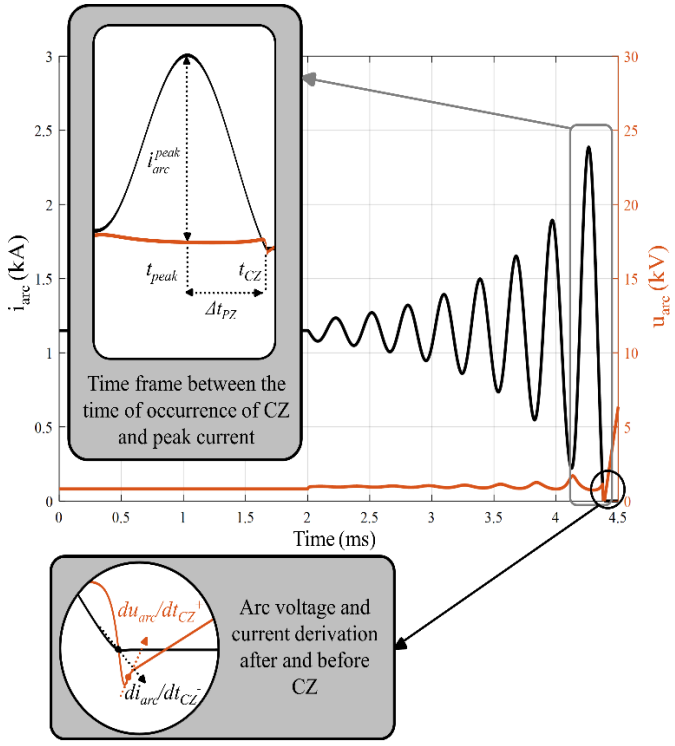

Fig. 7. The simulated arc voltage and current and magnified criteria with specified details. Parameters: i_{DC} =1.2 kA; C_{res}=20 μF; L_{res}=150 μH; r_{res}=1 mΩ; $P(g_{arc}) = 1.03 g_{arc}^{0.5}\ (MW)$; $\tau(g_{arc}) = 8.3 g_{arc}^{0.4}\ (\mu s)$.

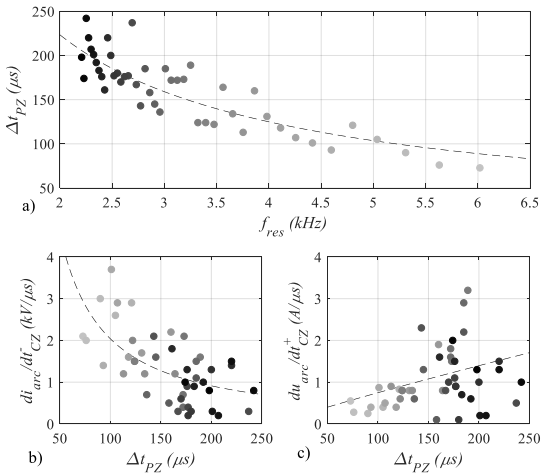

Fig. 8. (a) Time interval Δt_{PZ} as a function of resonance frequency (b)-(c) di_{arc}/dt_{CZ}^{-} and du_{arc}/dt_{CZ}^{+} as a function of time interval Δt_{PZ} (Faded circles refer to the higher frequency operation points).

The results as presented in Fig.8(a) indicate that the increase of the resonance frequency leads to a decrease in the time interval Δt_{PZ} and an increase in di_{arc}/dt_{CZ}^{-}. Accordingly, the arc may not be able to exchange thermal energy with the surrounding environment and fully adapt to the new condition. Therefore, it results in a thermal re-ignition, and a new arc is formed after a CZ. Fig .8(b) illustrates a negative correlation between the current deviation prior to CZ and the time interval. It is noted that faded circles/curves refer to the higher frequency operation points in this paper. The trend reemphasizes the decrease in the probability of successful interruption for a lower time interval with respect to a higher di_{arc}/dt_{CZ}^{-}.

In addition, the decrease of the resonance frequency causes an increase in Δt_{PZ} and the time lag between arc voltage and current. It results in more energy encapsulated in the CB leading to an increase du_{arc}/dt_{CZ}^{+}. Fig .8(c) illustrates the positive correlation between voltage derivation after CZ and the time interval. This trend confirms the decreased probability of successful interruption for a higher time interval with respect to a higher du_{arc}/dt_{CZ}^{+}.

As a result, while at high frequencies currents, the high current derivative can be identified as an effective factor in reducing the probability of successful interruption, a high voltage derivative plays an important role at low frequencies currents.

The precise capability curve based on the Schwarz model has been evaluated in the different frequency ranges and the time interval Δt_{PZ} as illustrated in Fig. 9. While the solid line refers to the imaginary part of the roots (ω_{res}) at different frequencies, the dash-point line indicates the real part of the roots (α_{res}). The overlapped region between the inside of the horizontal horseshoe ($\alpha_{PCZ} < \alpha_{res}$) and the frequency-band ($1/6\tau_0 < \omega_{res} < 1/5\tau_0$) is the desired operation region.

A desired range for di_{arc}/dt_{CZ}^{-} and du_{arc}/dt_{CZ}^{+} variations has been identified within 0.6-2.1 A/μs and 0.6-2.8 kV/μs, respectively for a successful interruption. Regarding the scatter of data, the average values of excitation frequency in these ranges have been calculated 3.2 kHz<f_{res}<3.9 kHz. Regarding Fig. 8, it is expected that the time lag between arc

current and voltage is long enough for compatibility of the arc in the resonance frequency range (or $5\tau_0 < \frac{1}{\omega_{res}} < 6\tau_0$).

Therefore, it could be stated that the critical time constant is located in this range as discussed in II.

As it can be concluded, the critical time constant τ_C could be kept within a particular range (between $5\tau_0$ and $6\tau_0$) for a successful interruption. Considering this point along with Fig. 9 reveals that in addition to the amplification factor, the resonance frequency plays a critical role to make a successful interruption. Accordingly, once the operation point is out of the frequency range, the probability of re-ignition increases.

It is noted that the defined criteria provide a connection with arc time constant τ_0 and help us to predict probable re-ignition based on arc current-voltage characteristics within one framework.

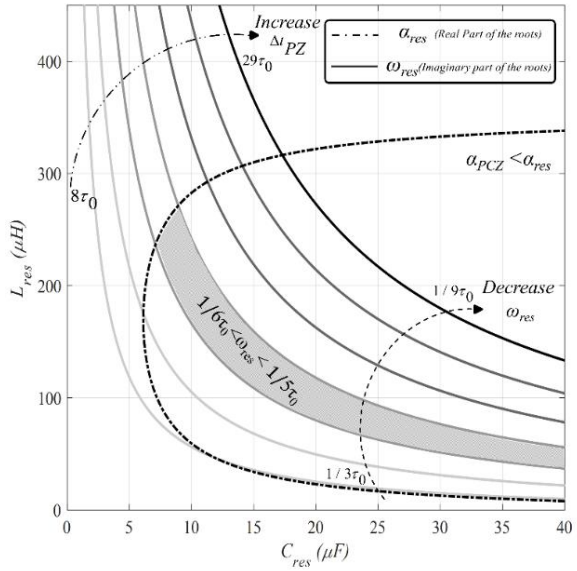

Fig. 9. The precise capability curve by considering different frequency range

The arc characteristic changes under the impact of external conditions such as pressure variation and transverse magnetic field and the type of gas. In response to this, the amplification coefficient (α_{res}) and the frequency of complex conjugate roots (f_{res}) have been calculated for the desired operation point (C_{res} = *20 μF* and L_{res} = *100 μH*) by variation of the arc time constant and cooling power (α=*0* and β=*0*). The sensitivity analysis by varied arc parameters is presented in Fig.10.

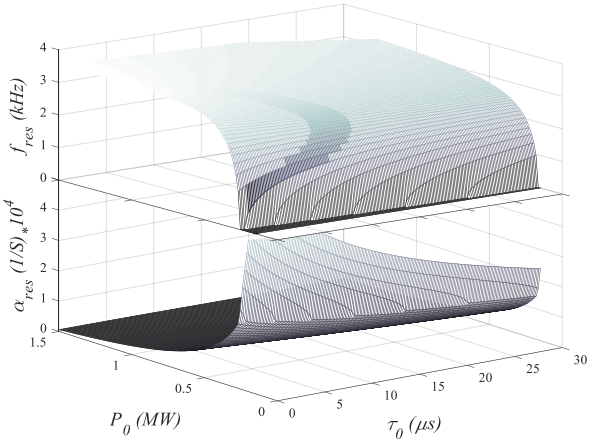

Fig. 10. The frequency and amplification coefficient corresponds with the complex conjugate roots at the desired operation point by variation the arc parameters

The bottom plot in Fig. 10 indicates that a higher arc time constant and cooling power constant leads to a decrease in the amplification coefficient. It can be interpreted in this way that an increase in arc parameters with respect to (1) leads to a reduction of the absolute value of the negative differential resistance ($|du_{arc}/di_{arc}|$).

The top plot in Fig. 10 indicates that the resonance frequency generally increases with the increasing either arc time constant or cooling power constant.

VI. Conclusion

DC interruption based on the passive circuit takes some limitation owing to the nature of arc in the case of high-currents including various frequency contents. However, regarding the low-cost and simplicity, PRBs are increasingly employed in multi-terminal HVDC networks as the transfer switching devices. Regarding the importance of the arc model in connection with the resonant circuit, this paper comprehensively investigated the arc model from static characteristic to dynamic characteristic. Accordingly, the modeling of the wall-stabilized and free burning arc based on the heuristic approach (GA) have been evaluated to identify the quasi-static and static characteristic of the arc. Moreover, the state-space model has been employed to analytically reveal the interaction of the dynamic arc model, the resonance circuit, and the interruption capability. In addition, a precise capability curve using a proposed dynamic arc model suitable for the arc voltage evaluation in different frequency ranges have been developed. Furthermore, the proper criteria for the assessment of the interruption capability have been defined to find the interruption failure origins in PRBs, and serving a safe frequency range for adjusting the shunt impedance to reach the maximum performance of mechanical CB. It is indicated that a desired range for di_{arc}/dt_{CZ}^- and du_{arc}/dt_{CZ}^+ variations were identified within 0.6-2.1 A/μs and 0.6-2.8 kV/μs, respectively dealing with a successful interruption. In addition, it is deduced that while the time derivative of the current is a prominent factor in high frequency arc current, the voltage derivation plays a significant role in the arc current with a lower frequency in a successful interruption.

The results help us to reach the maximum performance of PRBs within a safe and reliable operation of the mechanical breaker. In addition, it could be feasible to use the presented approach for a design improvement of the mechanical breaker through the precise capability curve and the interaction of the thermal criterion and cooling system. Furthermore, the results can applicable in the standardization and dielectric stress tests of future HVDC networks equipped with PRBs.

References

[1] C. Barker and P. Christensen, “HVDC Grid Feasibility Study Working Group B4.52 April 2013,” no. April, 2013.

[2] C. M. Franck, “HVDC Circuit Breakers: A Review Identifying Future Research Needs,” *IEEE Trans. Power Deliv.*, vol. 26, no. 2, pp. 998–1007, Apr. 2011, doi: 10.1109/TPWRD.2010.2095889.

[3] V. Lenz, “DC Current Breaking Solutions in HVDC Applications,”

2015, doi: 10.3929/ethz-a-010671622.
[4] M. Bonkarev, “Concept Analysis for High-Voltage Direct-Current Circuit Breakers for Application in a Network of HVDC Transmission,” no. April, p. 126, 2014.
[5] M. K. Bucher and C. M. Franck, “Fault Current Interruption in Multiterminal HVDC Networks,” *IEEE Trans. Power Deliv.*, vol. 31, no. 1, pp. 87–95, Feb. 2016, doi: 10.1109/TPWRD.2015.2448761.
[6] E. v Bonin, B. Koetzold, K. Möller, G. Oberdorfer, J. Schwarz, and H. G. Thiel, “A method of current interruption in HVDC networks by means of AC circuit-breaker with adapted arc characteristics and energy absorbers,” in *International Conf. on large high tension electric systems*, 1970, p. 15.
[7] H. Ekström Åand Härtel, H. P. Lips, W. Schultz, P. Joss, H. Holfeld, and D. Kind, “Design and testing of an HVDC circuit breaker,” in *Cigré session*, 1976, pp. 6–13.
[8] A. L. Courts, J. J. Vithayathil, N. G. Hingorani, J. W. Porter, J. G. Gorman, and C. W. Kimblin, “A new DC breaker used as metallic return transfer breaker,” *IEEE Trans. Power Appar. Syst.*, vol. PAS-101, no. 10, pp. 4112–4121, 1982, doi: 10.1109/TPAS.1982.317089.
[9] J. Vithayathil, A. Courts, W. Peterson, N. Hingorani, S. Nilsson, and J. Porter, “HVDC Circuit Breaker Development and Field Tests,” *IEEE Trans. Power Appar. Syst.*, vol. PAS-104, no. 10, pp. 2692–2705, Oct. 1985, doi: 10.1109/TPAS.1985.319110.
[10] B. Pauli, G. Mauthe, E. Ruoss, G. Ecklin, J. Porter, and J. Vithayathil, “Development of a high current HVDC circuit breaker with fast fault clearing capability,” *IEEE Trans. Power Deliv.*, vol. 3, no. 4, pp. 2072–2080, 1988, doi: 10.1109/61.194019.
[11] B. Bachmann, G. Mauthe, E. Ruoss, H. P. Lips, J. Porter, and J. Vithayathil, “Development of a 500kV Airblast HVDC Circuit Breaker,” *IEEE Trans. Power Appar. Syst.*, vol. PAS-104, no. 9, pp. 2460–2466, Sep. 1985, doi: 10.1109/TPAS.1985.318991.
[12] A. Lee, M. Ieee, J. Vithayathil, and F. Ieee, “IEEE Transactions on Power Apparatus and Systems, Vol. PAS-104, No. 10, October 1985,” no. 10, pp. 2721–2729, 1985.
[13] H. Ito *et al.*, “Instability of DC arc in SF/sub 6/ circuit breaker,” *IEEE Trans. Power Deliv.*, vol. 12, no. 4, pp. 1508–1513, Oct. 1997, doi: 10.1109/61.634168.
[14] H. Nakao *et al.*, “d.c. current interruption in HVDC SF6 gas MRTB by means of self-excited oscillation superimposition,” *IEEE Trans. Power Deliv.*, vol. 16, no. 4, pp. 687–693, 2001, doi: 10.1109/61.956757.
[15] M. M. Walter, “Switching Arcs in Passive Resonance HVDC Circuit Breakers,” no. 21548, p. 253, 2013, doi: 10.3929/ethz-a-010112102.
[16] M. M. Walter and C. M. Franck, “Influence of arc chamber parameters on passive resonance circuit of HVDC circuit breakers,” *CIGRE 2011 Bol. Symp. - Electr. Power Syst. Futur. Integr. Supergrids Microgrids*, pp. 1–7, 2011.
[17] R. P. P. Smeets, V. Kertész, and A. Yanushkevich, “Modelling and experimental verification of DC current interruption phenomena and associated test-circuits,” *CIGRE Sess. 45 - 45th Int. Conf. Large High Volt. Electr. Syst. 2014*, vol. 2014-Augus, pp. 1–13, 2014.
[18] L. Stefan and J. Bort, “Characterizing Axially Blown Arcs for Passive Oscillation DC Switches presented by,” no. 25852, 2019.
[19] M. Lindmayer, “Cooling Mechanisms of Switching Arcs under Transverse Magnetic Fields in Comparison with Arcs Without Magnetic Blast,” *IEEE Trans. Plasma Sci.*, vol. 46, no. 2, pp. 444–450, 2018, doi: 10.1109/TPS.2017.2788450.
[20] B. Xiang *et al.*, “DC Interrupting With Self-Excited Oscillation Based on the Superconducting Current-Limiting Technology,” *IEEE Trans. Power Deliv.*, vol. 33, no. 1, pp. 529–536, 2018, doi: 10.1109/TPWRD.2017.2718589.
[21] L. S. J. Bort, M. Vonesch, and C. M. Franck, “Controlling the differential resistance of axial blown arcs,” *J. Phys. D. Appl. Phys.*, vol. 52, no. 45, p. 455204, Nov. 2019, doi: 10.1088/1361-6463/ab34e0.
[22] C. M. Franck, R. Smeets, A. Adamczyk, H. Bahirat, and others, “Technical requirements and specifications of state-of-the-art HVDC switching equipment,” *CIGRÉ JWG A3/B4-34*, 2017.
[23] M. M. Walter and C. M. Franck, “Optimal test current shape for accurate arc characteristic determination,” *IEEE Trans. power Deliv.*, vol. 29, no. 4, pp. 1798–1805, 2014.
[24] M. Walter and C. Franck, “Improved method for direct black-box arc parameter determination and model validation,” *IEEE Trans. Power Deliv.*, vol. 29, no. 2, pp. 580–588, 2014, doi: 10.1109/TPWRD.2013.2283278.
[25] N. A. Belda and R. P. P. Smeets, “Test Circuits for HVDC Circuit Breakers,” *IEEE Trans. Power Deliv.*, vol. 32, no. 1, pp. 285–293, 2017, doi: 10.1109/TPWRD.2016.2567783.
[26] N. A. Belda, C. A. Plet, and R. P. P. Smeets, “Full-Power Test of HVDC Circuit-Breakers With AC Short-Circuit Generators Operated at Low Power Frequency,” *IEEE Trans. Power Deliv.*, vol. 34, no. 5, pp. 1843–1852, 2019, doi: 10.1109/tpwrd.2019.2910141.
[27] N. A. Belda, R. P. P. Smeets, and R. M. Nijman, “Experimental Investigation of Electrical Stresses on the Main Components of HVDC Circuit Breakers,” *IEEE Trans. Power Deliv.*, vol. 8977, no. VI, pp. 1–1, 2020, doi: 10.1109/tpwrd.2020.2979934.
[28] L. Vinet and A. Zhedanov, “A ‘missing’ family of classical orthogonal polynomials,” *Antimicrob. Agents Chemother.*, vol. 58, no. 12, pp. 7250–7257, Nov. 2010, doi: 10.1088/1751-8113/44/8/085201.
[29] J. L. Zhang, J. D. Yan, and M. T. C. Fang, “Electrode evaporation and its effects on thermal arc behavior,” *IEEE Trans. Plasma Sci.*, vol. 32, no. 3 II, pp. 1352–1361, 2004, doi: 10.1109/TPS.2004.827606.
[30] K. Niayesh and M. Runde, *Power Switching Components*. Cham: Springer International Publishing, 2017.